Chapter 6
Scatterometer's Unique Capability in Measuring Ocean Surface Stress

W. Timothy Liu, Xiaosu Xie, and Wenqing Tang

6.1 Introduction

Ocean surface stress, the turbulent transfer of momentum between the ocean and the atmosphere, is a vector quantity with a magnitude and a direction. It is closely related to wind but not solely driven by wind, as it depends also on ocean parameters such as surface current and temperature. While the general public appreciates wind as air in motion, very few people know what is stress. Even for oceanographers, the concept of stress distribution is largely derived from that of wind, because there was no large-scale measurement of stress over the ocean until the launch of the first scatterometer. A scatterometer measures the ocean surface roughness that is supposed to be in equilibrium with stress, and therefore it has the unique capability of measuring stress over the global ocean.

Although scatterometer measurements were related to stress, in prelaunch studies of the first scatterometer on Seasat (e.g. Wentz, 1978; Jones and Schroeder, 1978), and were validated against stress measurements (Liu and Large, 1981), scatterometers have been promoted as wind measuring instruments for the past 3 decades. The geophysical product of the scatterometer is the equivalent neutral wind (U_N). U_N, by definition, has an unambiguous relation with surface stress, provided that ocean surface current is negligible, while the relation between actual wind and surface stress depends also on atmospheric density stratification (see Section 6.2). Over most of the ocean, the atmosphere is generally believed to be near neutral, current speed is much smaller than wind speed, and U_N is assumed to be the actual wind, particularly in operational weather prediction.

Wind over ocean is much needed for marine weather forecast and to avoid shipping hazard. The significance of wind measurement is clearly felt, for example, when a hurricane suddenly intensifies and changes course or when the unexpected delay of monsoon brings drought. Surface wind convergence brings moisture and latent heat that drives deep convection and fuels atmospheric circulation. Detailed

W.T. Liu (✉)
Jet Propulsion Laboratory, California Institute of Technology, Pasadena, CA 91109-8099, USA
e-mail: w.t.liu@jpl.nasa.gov

V. Barale et al. (eds.), *Oceanography from Space*,
DOI 10.1007/978-90-481-8681-5_6,

distribution of wind power is also needed for the optimal deployment of floating wind farms in open sea that are enabled by new technology (Liu et al., 2008a). Just a few decades ago, almost all ocean wind measurements came from merchant ships. However, the quality and geographical distribution of these wind reports were uneven. Today, operational numerical weather prediction (NWP) also gives us wind information, but NWP depends on models, which are limited by our knowledge of the physical processes and the availability of data. The scatterometers have provided observations for important science and operational applications, in the past decades, as reviewed by Liu (2002) and Liu and Xie (2006). At this tenth anniversary of QuikSCAT launch, we will go back to the basics of scatterometry and turbulence transfer to demonstrate the uniqueness of scatterometer stress measurements that may enable new scientific applications from new perspectives.

For oceanographers, it is stress more than wind that directly drives ocean circulation. The two-dimensional stress field is needed to compute the divergence and curl (vorticity) that control the ocean vertical mixing. The mixing brings short-term momentum and heat trapped in the surface mixed layer into the deep ocean, where they are stored over time. It also brings nutrients and carbon stored in the deep ocean to the surface, where there is sufficient light for photosynthesis. Horizontal currents, driven in part by stress, distribute the stored heat and carbon in the ocean. The magnitude of stress affects the turbulent transfer between ocean and atmosphere of heat, moisture and gases that are critical for climate changes.

The relation between wind and stress, affecting the interpretation of scatterometer measurements, will be described in Section 6.2. Talking about measuring stress with a scatterometer, but using U_N as the actual wind, and explaining the variation of scatterometer observations from wind theories, would lead to a misinterpretation of physical processes. Hence, the difference between wind and stress is tackled in Section 6.3. Using a neutral drag coefficient to derive stress from the U_N provided by the scatterometer has inherent deficiency, so a new geophysical model function (GMF) to retrieve stress is discussed in Section 6.4. With the potential benefit of direct retrieval of stress, which is also driven by smaller-scale ocean surface parameters such as current and temperature, a re-thinking of the feedback processes is explored in Section 6.5. A constellation of scatterometers to meet operational and research needs is presented in Section 6.6.

6.2 Turbulence Parametrization and Scatterometer Geo-Physical Product

Ocean surface stress (τ) is the turbulent transfer of momentum between the ocean and the atmosphere. The turbulence is generated by atmospheric instability caused both by wind shear (difference between wind and current) and buoyancy (vertical density stratification resulting from temperature and humidity gradients). In the past, direct τ measurements, by the so-called eddy-correlation method, have only been done in a few field campaigns (Smith, 1980). In practice, knowledge of τ is derived

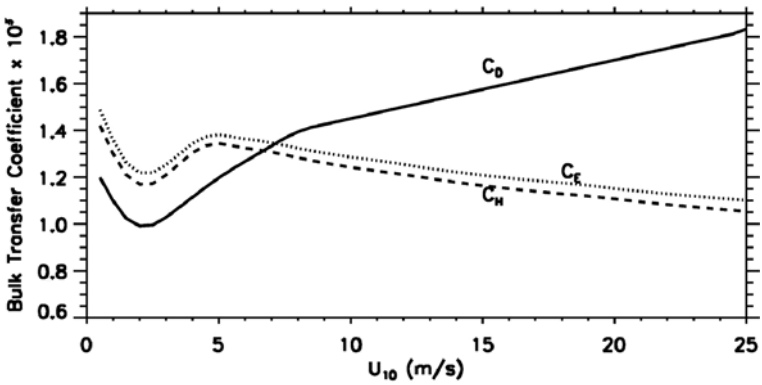

Fig. 6.1 Variation of the bulk transfer coefficients of momentum (drag coefficient), heat, and moisture with wind speed by Liu et al. (1979)

from winds (U) at a reference height, through a drag coefficient C_{D}, as defined by

$$\tau = \rho C_{\mathrm{D}} \left(U - U_{\mathrm{S}}\right)^2 \tag{6.1}$$

where U_{s} is the surface current and ρ is the air density. C_{D} has been derived largely from field measurements (Kondo, 1975; Smith, 1980; Large and Pond, 1981). Figure 6.1 (Liu et al., 1979) illustrates the variation of C_{D} with wind speed, at neutral stability, compared with the transfer coefficient for heat (C_{H}) and water vapor (C_{E}). At low wind speed ($U < 3$ m/s), the flow is smooth and C_{D} increases with decreasing wind speed. At moderate wind ($3 < U < 25$ m/s), C_{D} is an increasing function of wind speed for a rough sea with open fetch.

The drag coefficient is, of course, only a simple approximation to relate what we want – stress, to the measurement that is available – wind. We imbed our insufficient knowledge of turbulence transfer in this coefficient. Secondary factors, such as sea states, swell, and spray from breaking waves (e.g. Donelan et al., 1997; Bourassa et al., 1999), whose data are not generally available, are not included in this parameterization schemes and should be part of the errors. Although we include surface current in the formulation (Equation 6.1), it is generally ignored because no current measurement is readily available. These factors, together with the stability effects may contribute to the uncertainties of the drag coefficient.

Liu et al. (1979) first proposed a parameterization method of stress, which is equivalent to a C_{D} including the stability effects and molecular constraints at the interface, by solving the similarity equation (non-dimensional flux-profile relation) in the surface layer, where the vertical gradient of stress is negligible:

$$\frac{U - U_{\mathrm{S}}}{U_*} = 2.5\left(\ln\frac{z}{z_0} - \psi_{\mathrm{u}}\right) = \frac{1}{\sqrt{C_{\mathrm{D}}}}, \tag{6.2}$$

where $U_* = (\tau/\rho)^{1/2}$ is the friction velocity, z_0 is the roughness length, and ψ_u is a function of the stability parameter, which is the ratio of buoyancy to shear

production of turbulence. Equation (6.2) is solved simultaneously with similarity equations for temperature and humidity. An alternative to using the neutral C_D is to express z_0 as a function of U_*. For example, Liu and Tang (1996) incorporated such a relation in solving the similarity equation. They combined a smooth flow (Nikuradse, 1933) and rough flow (Charnock, 1955) relations to give

$$Z_0 = 0.11\frac{\nu}{U_*} + 0.011\frac{U_*^2}{g} \tag{6.3}$$

where ν is the kinematic viscosity and g is the acceleration due to gravity.

Typical wind profiles at various stabilities are shown in Fig. 6.2 as illustration. Neglecting U_s and ψ_u in Equation (6.2), U becomes U_N and it is uniquely related to U_* (or τ). Although the atmosphere is believed to be near neutral over most ocean area, exact neutral stability ($\psi_u = 0$) is rare, and to compute U_N from conventional wind measurements of U (point A in Fig. 6.2), the stability effect has to be removed. First, U_* and z_0 are computed based on the parameterization scheme of Liu et al. (1979) (the computer codes and subsequent modifications were presented by Liu and Blanc, 1984; Liu and Tang, 1996), as the slope and intercept at the surface of the curve in Fig. 6.2. The neutral relation (straight line) defined by U_* and z_0 will then give U_N (point B). This method has been used in development and calibration of all the GMF of the NASA scatterometer.

Liu et al. (1979) first postulated that, in a rough sea, under a moderate range of winds, C_H and C_E do not increase with wind speed because molecular constraint

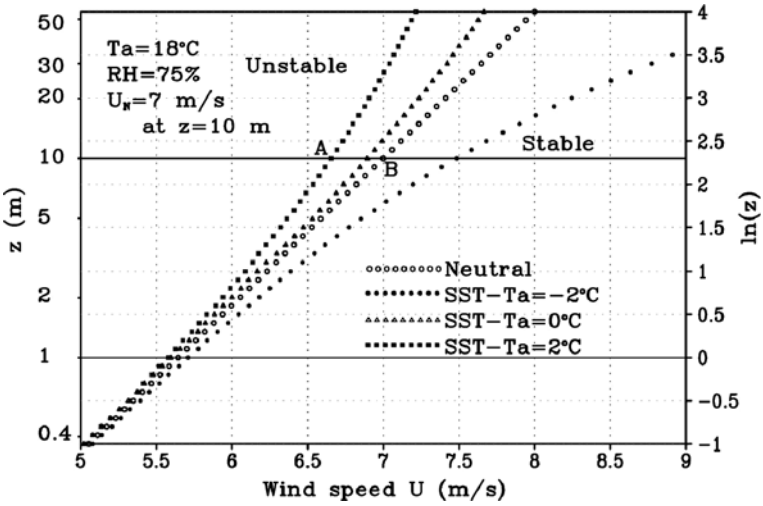

Fig. 6.2 Typical wind profiles at various stability conditions derived from the flux-profile relation by Liu et al. (1979). B is the equivalent neutral wind corresponding to the actual wind measurement at A

at the interface, while C_D may still increase since momentum is transported by form-drag. The heat and moisture transfer coefficients are defined by

$$H = \rho c_P C_H (T - T_s)(U - U_S) \tag{6.4}$$

$$E = \rho C_E (Q - Q_s)(U - U_S) \tag{6.5}$$

where c_P is the isobaric specific heat, H is the heat flux, E is moisture flux (evaporation). T is the potential temperature, T_s the sea surface temperature, and Q is the specific humidity at a reference level and Q_s is the specific humidity at the interface. Liu's hypothesis on C_H and C_E, up to 20 m/s wind speed, as illustrated in Fig. 6.1, was subsequently supported by measurements in field experiments (e.g. DeCosmo et al., 1996).

Emanuel (1995) argued, from theoretical and numerical model results, that the scenario of Liu et al. (1979) could not be extrapolated to the strong wind regime of a hurricane. To attain the wind strength of a hurricane, the energy dissipated by drag could not keep increasing while the energy fed by sensible and latent heat does not increase with wind speed. His results, showing that the maximum wind speed in mature storm is sensitive to ratio of C_H and C_E to C_D, and that the ratio could not exceed a very small range, put limit on the increase of C_D as a function of wind speed.

Under strong winds, flow separation occurs, and wind is detached from roughness growth. The postulation of the level-off of the increase of C_D with wind speed at hurricane scale winds was supported by the results of the laboratory studies of Donelan et al. (2004), and the aircraft experiments by Powell et al. (2003) at wind speed above 30 m/s, as illustrated in Fig. 6.3. The result of Large and Pond (1981) derived for the range of moderate wind speeds is extrapolated to the range of strong wind speeds for comparison in the figure. Such flow separation may explain the high wind saturation of the scatterometer discussed in Section 6.3.2.

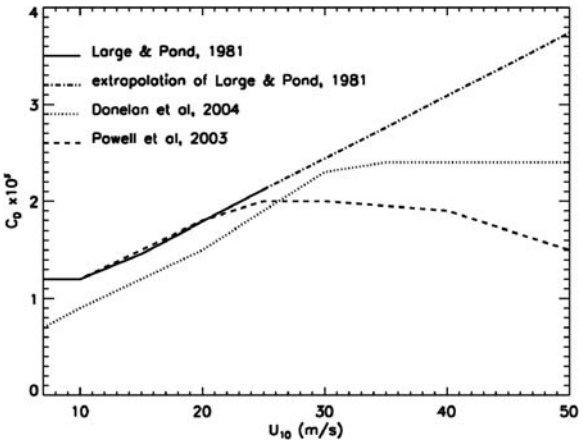

Fig. 6.3 Variation of the drag coefficients in strong winds

6.3 Characterization of Stress Versus Wind Distribution

6.3.1 Dependence on Surface Temperature and Current

When the first Quick Scatterometer (QuikSCAT) data came back in 1999, the science team was surprised to see that the scatterometer signal in the equatorial Pacific propagates westward with the ocean temperature front of the tropical instability waves, in the area where we expected to see steady trade winds (e.g. Liu et al., 2000; Chelton et al., 2001). Such coincident propagation was previously observed by Xie et al. (1998) in European Research Satellite (ERS) data. Since then, the spatial coherence between scatterometer measurements and sea surface temperature (T_s) has been observed over many locations and under various atmospheric conditions, e.g. over the Kuroshio Extension (e.g. Nonaka and Xie, 2003), over the circumpolar current (e.g. O'Neill et al., 2003), Indian Ocean (Vecchi et al., 2004), in the East China Sea during winter cold air outbreak (Xie et al., 2002), over the Gulf Stream Ring (Park and Cornillon, 2002), and over typhoon wake (Lin et al., 2003). Following traditional paths to study atmospheric boundary layer processes, many scientists were quick to postulate explanations of the wind and T_s correlation, based on boundary layer height change, pressure gradient force, secondary flow, cloud entrainment, and organized convection, but none of these is generally applicable to the ubiquitous correlation, as pointed out in the review by Small et al. (2008).

The first explanation by oceanographers, when they saw the results of Liu et al. (2007) showing that QuikSCAT measurements deviate from the mean winds with rotation in opposite direction to the underlying surface current of the Agulhas Extension meanders, was that either the drifter (current) or the scatterometer measurements were erroneous. Their reasoning was that the strong current meanders should impart its rotation on the prevailing westerly wind through drag, and the wind anomalies should show the same rotation as the current. Misinterpreting scatterometer stress as wind is the cause of confusion. Stress must be spatially coherent with T_s and ocean current, which create buoyancy and wind shear. As pointed out by Liu et al. (2007) and Liu and Xie (2008), at small turbulence scales at the surface, factors that affect atmospheric boundary layer dynamics (wind), such as Coriolis force, pressure gradient force, baroclinicity, cloud entrainment, etc., are not important. That is why the spatial coherence is ubiquitous, under all kinds of atmospheric circulations. Stress is the vector difference between wind and current. For a uniform wind blowing over a rotating current, the vector differences will have opposite rotation to the current (Park et al., 2006). The ocean signals, of course, will affect winds aloft through stress. The dynamic factors will then become important.

Liu et al. (2007) observed T_s signatures in cloud and atmospheric temperature high in the atmosphere over the Agulhas Extension. Even stronger penetrating signals have been found, not only in temperature profiles but also in precipitation profiles over the Kuroshio Extension. Present numerical models of atmospheric circulation in the mid-latitudes do not propagate the surface stress signal vertically much beyond the atmospheric boundary layer. The observations posted a challenge

to understanding the transition from random turbulence to organized convection in the atmosphere.

The difference between winds and stress over oceanfronts is well documented by Liu et al. (2007) for the Agulhas Extension and by Liu and Xie (2008) for the Kuroshio Extension. Figure 6.4 shows the results of a conceptual experiment over the Kuroshio Extension by Liu and Xie (2008). A uniform wind field (average U_N speed blowing from west to east) over the area covered by the current meanders is assumed, with high and low T_s anomaly centers measured by the Advanced Microwave Scanning System – Earth Observing System (AMSR-E) marked as ° and * respectively.

U_N is computed with the stability-dependent bulk parameterization scheme of Liu et al. (1979), using air temperature from the National Center for Environmental Prediction (NCEP). The coherence between U_N and T_s is obvious even for a uniform wind field (Fig. 6.4a). The U_N computed from a uniform wind field shows the same

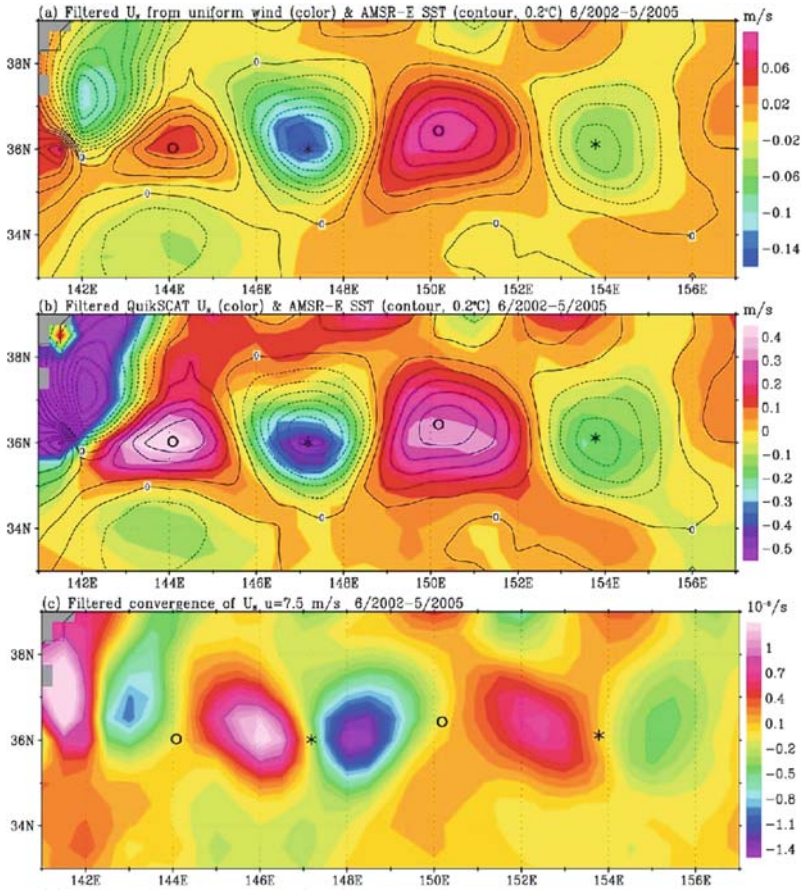

Fig. 6.4 (continued)

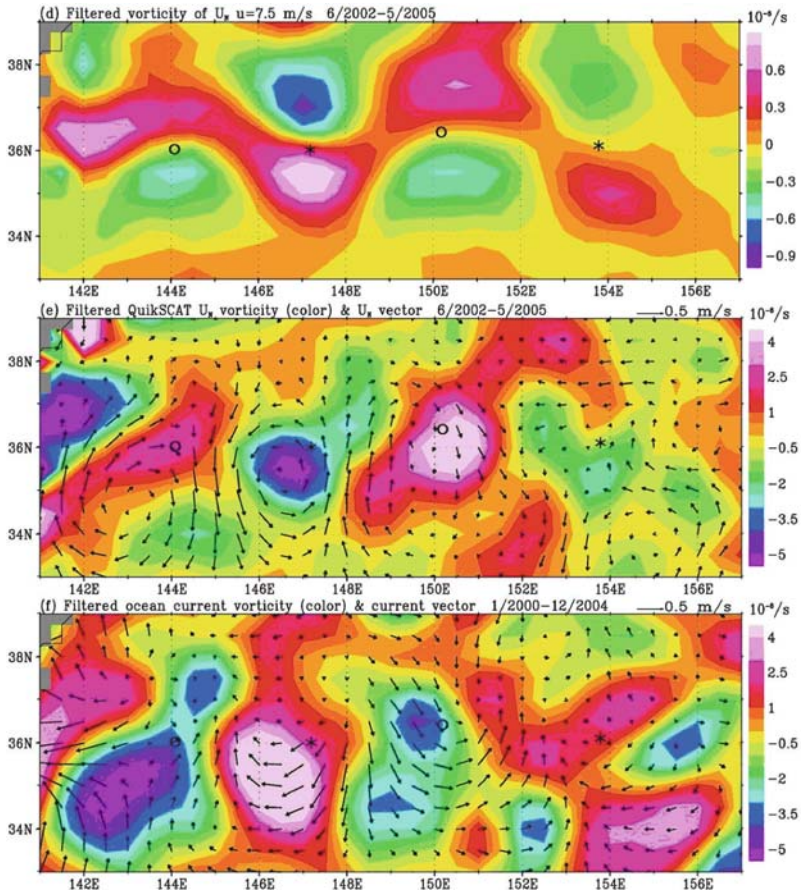

Fig. 6.4 (**a**) Isotherms of filtered *T*s measured by AMSR-E (0.2°C interval) superimposed on filtered U_N computed from a uniform wind field of $u = 7.5$ m/s (color, m/s). *Solid* and *broken lines* represent positive and negative values, respectively. (**b**) Same as (**a**), except for filtered magnitude of QuikSCAT U_N (*color*, m/s). (**c**) Convergence of filtered U_N computed from the uniform wind (unit is 10^{-6}/s). (**d**) Vorticity of filtered U_N computed from the uniform wind (unit is 10^{-6}/s). (**e**) Filtered vector (*black arrows*) superimposed on vorticity (color, 10^{-6}/s) of U_N observed by QuikSCAT. (**f**) Filtered vector (*black arrows*) superimposed on vorticity (color, 10^{-6}/s) of the surface current measured by Lagrangian drifters. The large-scale gradients are removed by a two-dimensional filter

coherent pattern as that measured by QuikSCAT (Fig. 6.4b). Figure 6.4c shows that the convergence of U_N computed from the uniform wind field is in quadrature (90° phase difference) with T_s in the downwind direction, implying that the convergence is in-phase with the downwind T_s gradient.

A similar spatial coherence is observed between T_s and QuikSCAT U_N convergence. Figure 6.4d shows that the vorticity of the computed U_N is in quadrature with T_s in the crosswind direction; vorticity is in-phase with the crosswind T_s gradient. Positive vorticity is found to the south and negative anomalies to the north

of the cold eddy, and vice versa for the warm eddy. QuikSCAT should observe the vorticity distribution, if there is no ocean current (e.g. O'Neill et al., 2003), but its observations do not show such crosswind relation (Fig. 6.4e). Positive vorticity is collocated (in-phase) with warm water and negative vorticity is collocated with cold water. The vorticity of the observed U_N is opposite to the vorticity of the surface current measured by drifters (Fig. 6.4f), confirming scatterometers measure the vector difference between wind and current, as associated with stress. Liu et al. (2007) found similar results over the Agulhas Extension.

The stability effect on the difference between wind and stress, in the form of the difference between U_N and U, is governed by ψ_u, as

$$\delta U = U_N - U = 2.5 U_* \psi_u \tag{6.6}$$

Using U_N provided by QuikSCAT, sea surface temperature from AMSR-E, air temperature and air humidity from the reanalysis of the European Center for Medium-Range Weather Forecasts (ECMWF), Liu et al. (2010) computed δU at 10 m averaged over a 3 years period, for January and July (as shown in Fig. 6.5). This distribution of the stability effect on wind speed follows closely the distribution of sea-air temperature difference shown in Fig. 6.6. Because atmospheric temperature

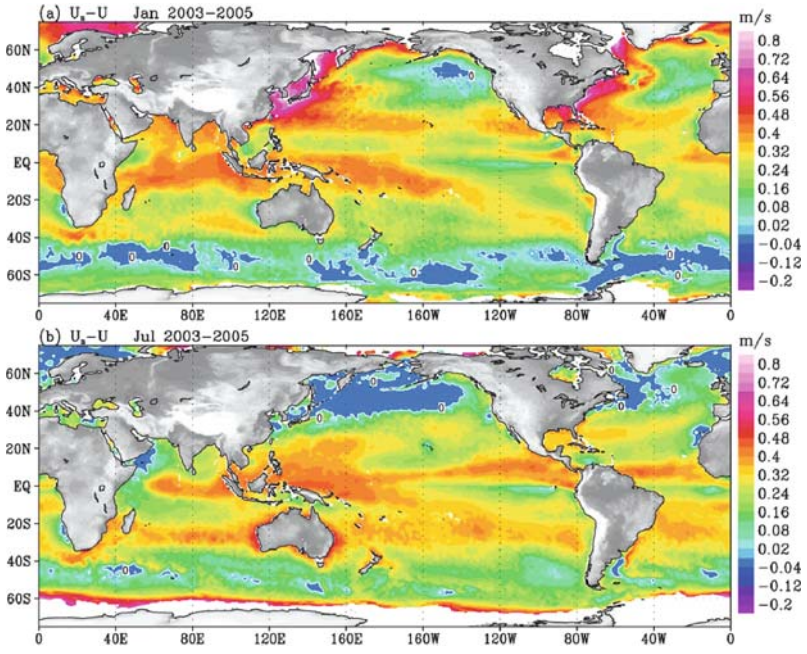

Fig. 6.5 Difference between equivalent neutral wind and actual wind at 10 m for (**a**) January and (**b**) July

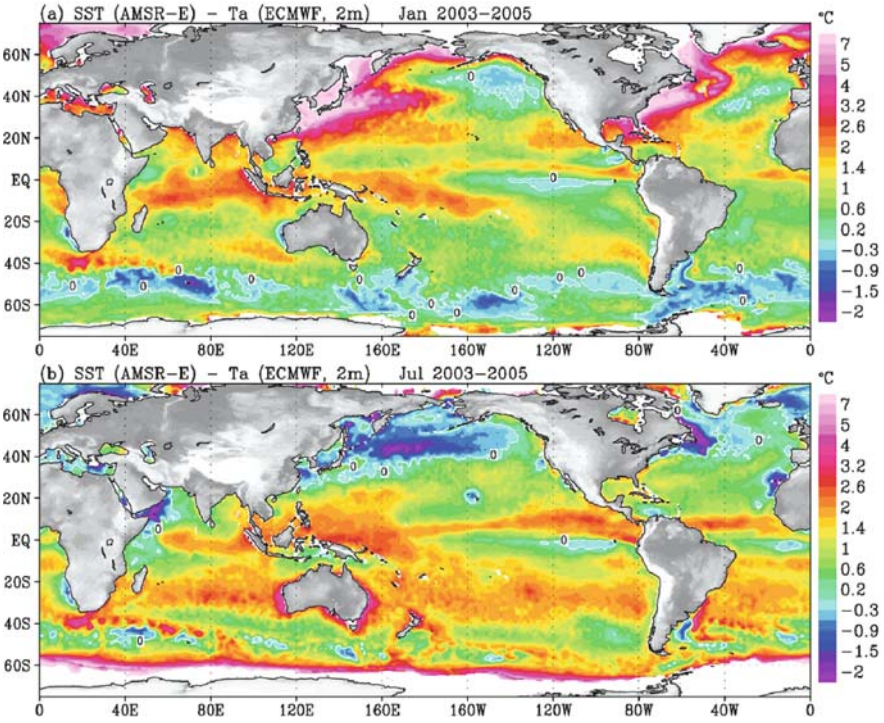

Fig. 6.6 Difference between sea surface temperature and air temperature (2 m) for (**a**) January and (**b**) July

variations have larger scale than oceanic temperature variations, the buoyancy-generated turbulence should have strong spatial correlation with T_s at small scales.

The formulation of ψ_u was largely based on experiment data on land, validated only with small amount of measurements over ocean. Although there have been many investigations to improve flux parameterization, (e.g. Fairall et al., 1996) in the past few decades, there is no significant change in the formulation of ψ_u. As shown by Liu et al. (2007) and Liu and Xie (2008), and discernable in Fig. 6.4, the dynamic range of U_N over T_s anomalies computed from uniform wind fields is smaller than the QuikSCAT measurement. One of the plausible reasons is that the ψ_u in use now underestimates the stability effect on vertical wind speed changes, and needs to be investigated. Another reason is a positive atmospheric feedback through convection (see Liu et al., 2007; Liu and Xie, 2008).

Although both NCEP and ECMWF have assimilated QuikSCAT data since 2002, the data were assimilated as actual wind vector and not stress. The wave-number spectra constructed from ECMWF 10 m winds collocated with one swath of QuikSCAT data on August 25, 2005, over the Atlantic (Fig. 6.7) shows that QuikSCAT U_N has higher power than the ECMWF winds at high wave numbers.

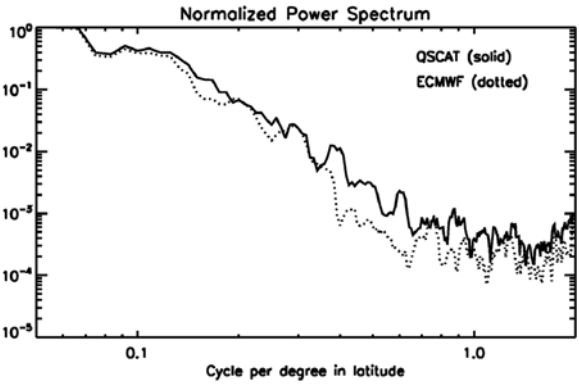

Fig. 6.7 Power spectrum of UN measured by QuikSCAT and 10 m wind from ECMWF

It implies that the stress measured by QuikSCAT has more small-scale information than the winds provided by ECMWF, unless the comparison reflects the deficiency in the models.

6.3.2 High Wind Saturation

Engineers have long been puzzled by the high wind saturation of scatterometer measurements causing an underestimation of the strength of winds in tropical cyclones and extratropical storms by scatterometers (see review in Liu and Xie, 2006). Retrieving strong winds from scatterometer observations is known to be difficult because of the lack of in-situ standards for calibration. The problem is clearly illustrated in Fig. 6.8, where QuikSCAT measurements at Ku-band are compared with collocated HWind speed operationally produced by the Hurricane Research Division at the Atlantic Oceanographic and Meteorological Laboratory, at 1 m/s bin size (Liu, 2010). Data for the 12 hurricanes of the North Atlantic in the 2005 seasons, excluding those with over 10% chances of rain, were examined. Figure 6.8 shows that, in moderate winds ($U < 35$ m/s), the logarithm of the backscatter (in term of the normalized radar cross section σ_0 in dB) increases linearly with the logarithm of wind speed, at both polarizations.

The error bar (one standard deviation of the 1 m/s wind speed bin) is mainly due to the dependence on azimuth angle (see Section 6.4). At strong winds ($U > 35$ m/s), however, σ_0 increases at a much slower rate with increasing wind speed. Errors increase because there is a small number of data in the high speed bins. Similar saturation is found in the C-band European Advanced Scatterometer (ASCAT). Strong wind saturation has been postulated (e.g. Donelan and Pierson, 1987) and observed from aircraft in hurricane experiments (Donnelly et al., 1999; Yueh et al., 2000).

When the model function developed over the moderate wind range is applied to the strong winds, an underestimation of wind speed results. Efforts have been made to adjust the model function (slope in Fig. 6.8) in strong winds and to find a sensor channel (combination of polarization, frequency, incident angle) for future

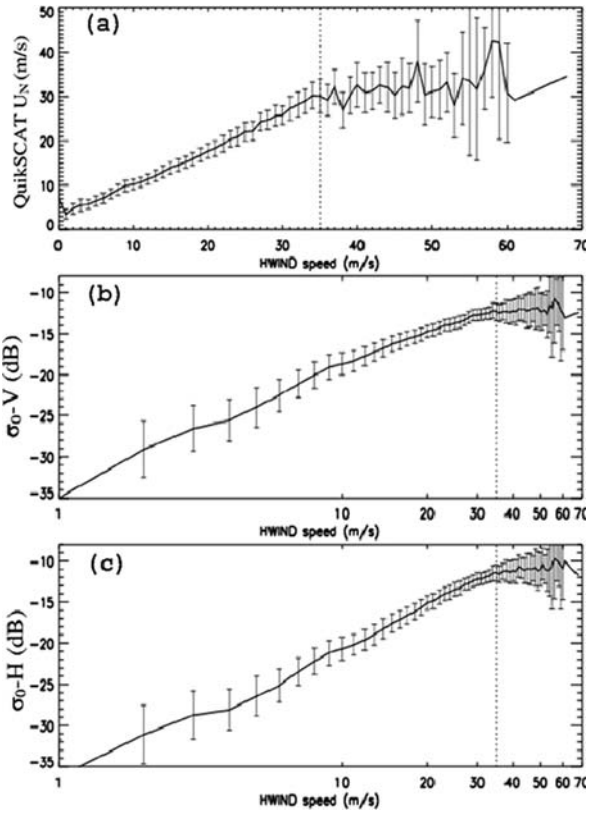

Fig. 6.8 Bin-average of (**a**) U_N, (**b**) normalized radar cross section at vertical, and (**c**) horizontal polarization measured by QuikSCAT for 12 hurricanes as a function of co-located Hwind. Error bars represent 1 standard deviation of data in each bin

scatterometers that would be sensitive to hurricane-scale winds (Esteban-Fernandez, 2006). As seen in Section 6.2, flow separation occurs at high winds and conventional formulations of drag coefficient fail. Although retrieving the very strong winds of a hurricane may not be an important and practical way to use the scatterometer, its measurements are significant not only in revealing the relation between wind and stress, but also in studying oceanic feed back to the dynamic forcing that is critical in hurricane maintenance and intensification.

6.4 Geophysical Model Function for Stress Retrieval

6.4.1 Equivalent Neutral Wind Retrieval

At present, QuikSCAT geophysical retrieval is through GMF-W, which relates the scatterometer normalized radar cross-section σ_0 with U_N, as

$$\sigma_0 = f\,(U_N, \chi, \vartheta, p) \tag{6.7}$$

where χ is the relative azimuthal angle between the plane of incidence of the radar beam and the wind direction, θ is the incidence angle (relative to nadir) and p represents the polarization. At fixed χ, σ_0 (in dB) increases approximately linearly with log (U_N). The azimuthal variation of σ_0 can be characterized as harmonics with "upwind-downwind asymmetry" and "up- wind-crosswind modulation". It has been demonstrated that the azimuthal angle dependence can be separated from the incidence angle and U_N functions using the 3-term Fourier series (Wentz et al., 1984; Freilich, 1996):

$$\sigma_0 = A_0\,(U_N,\theta) + A_1\,(U_N,\theta)\cos(\chi) + A_2\,(U_N,\theta)\cos(2\chi) \tag{6.8}$$

The core of GMF-W is consisted of the A coefficients as tabulated empirical data. The forward GMF-W accepts U_N vector as input and gives σ_0 as output. The inverse GMF, however, is not unique. A single measurement of σ_0 generates a range of potential wind vectors, all of which would have given rise to the observed backscatter. To solve the inverse problem, σ_0 at multiple azimuth angles are used. At least three collocated observations of σ_0 differing in "look", i.e. geometry (χ, θ), allows the determination of a unique wind vector. Theoretically, the solution could be found from data without noise. Noise complicates the solution and a maximum likelihood estimator (MLE) has to be used (Pierson, 1984). A common practice is to keep several ambiguous solutions at each wind vector cell. In order to select the proper ambiguity, we assume that the wind is unlikely to shift radically from one cell to the next and a median filter technique has been used (Shaffer et al., 1991). The median filter technique is an iteration procedure generally initialized by the NWP field in the so called "nudging".

6.4.2 Stress Retrieval

There are many reasons for a GMF-S to retrieve stress (or U_*) directly rather than the present GMF-W to retrieve U_N. A first reason lies in the present GMF-W, which should be developed and calibrated with U_N computed from research-quality in-situ wind measurements, using methods based on the similarity relations of Liu et al. (1979), as in Section 6.2. Indeed, such computation of U_N was performed before credible ocean surface wind products became available from operational NWP centers. Most of the tuning of the revised GMF after Seasat was based on NWP products (e.g. Wentz and Smith, 1999) that are not U_N (not corrected for stability dependence). The resulting errors are not reversible and difficult to gauge.

Ideally, stress could be derived from U_N retrieved from scatterometer, using a neutral drag coefficient. However, if the drag coefficient is not the same as that used to derive U_N for development of the GMF, an error will be introduced through the uncertainty of the drag coefficient. This is the second reason for a GMF-S. Weissman and Graber (1999) provide an example of the very few attempts to tabulate stress instead of U_N in the A coefficients of Equation (6.8). Two additional

reasons are related to the directional difference between wind and stress. The procedure to "select" the stress from multi-solutions with ambiguous direction needs modification in two steps. The first is testing various "nudging" fields that are more relevant to stress than wind. Our feasibility studies suggest that such changes in the nudging field is significant in the region where strong ocean current exists and stress should point to the direction of the vector difference between wind and current. A more flexible median filter should also be designed to accommodate the small spatial scale of stress as compared with winds.

The development of GMF-S could follow closely those for GMF-W, and our feasibility study using a small sample of stress vectors and "nudging" data that include ocean current are successful. One of the reason usually given for promoting scatterometer as a wind sensor instead of stress sensor is that there are more wind than stress measurements to develop and calibrate the GMF. Such explanation runs in contrast to the rationale behind using U_{N} as the geophysical product because of its unambiguous relation to stress. To provide each U_{N} for development or calibration the GMF from measured wind, stress or U_* has to be computed first as discussed in Section 6.2. There are as many stress available as U_{N}.

The stress prepared from wind in such way is not ideal because it addresses only the stability problem but does not include current information. Such deficiency may be somewhat alleviated through the ambiguity removal process by using more appropriate filter size and nudging with the vector difference between wind and optimal surface current information that is available. Ocean surface current measurements are very sparse. The current velocity has been derived from Argos satellite collections of the displacements of drifters with drogues centered at 15 m-depth (Niiler, 2001). Ocean surface currents are also provided by the Ocean Surface Currents Analyses – Realtime program, using a combination of scatterometer and altimeter data (Lagerloef et al., 1999). Global, high frequency current data are only available from numerical models, such as, Estimating the Circulation and Climate of the Ocean (Fukumori, 2002) and Regional Ocean Modeling System (Chao et al., 2009).

6.5 Potential Oceanic Feedback

Although Pacanowski (1987) showed the importance of the feedback of ocean current on stress in a numerical experiment more than two decades ago, many ocean scientists are still forcing their ocean models using stress that is entirely determined from the wind field, independent of local changes caused by ocean. With the availability of QuikSCAT data, Polito et al. (2001) discussed the surface current and temperature feedback to the stress forcing, and Pezzi et al. (2004) demonstrated negative feedback with ocean general circulation model, at the tropical instability waves. With the recent demonstration of spatial coherence between scatterometer measurement and T_{s} over extensive ocean regions, as discussed in Section 6.3, many numerical studies of T_{s} feedback to stress forcing were performed with numerical models (e.g. Seo et al., 2007; Spall, 2007; Hogg et al., 2009). The measurement of

stress field that depends not only on the fast and large-scale atmospheric circulation but also on the small scale and slow ocean processes as reflected in surface current and temperature will enable new studies from new perspective in the near future.

6.6 Satellite Constellations

One polar-orbiting scatterometer at a low altitude (e.g. 800 km) orbit, can sample at a location on Earth not more than two times a day. The temporal sampling may not be sufficient to monitor wind/stress with high frequencies. Meso-scale weather system, such as hurricane may be missed through orbit gaps. Additional instrument flying in tandem will allow the description of higher temporal variability and the reduction of the aliasing (bias introduced by sub-sampling) of the mean wind/stress, as described by Lee and Liu (2005) in their study on the impact on ocean mixed layer depth.

Besides QuikSCAT, there are two more scatterometers in operation. One is the C-band and fan-beam ASCAT on board the Meteorological Operational Satellite (METOP), launched in October 2006 by the European Space Agency. It has dual swath separated by a broad nadir gap. The other is a Ku-band, pencil beam, conically scanning scatterometer on Oceansat-2, launched in September 2009 by the Indian Space Agency.

The local time of ascending node for the three scatterometers is 5:54 AM, 9:30 PM, and noon, respectively. Figure 6.9 shows that the zonal average of revisit interval decreases from the equator to the poles because the orbits come closer at

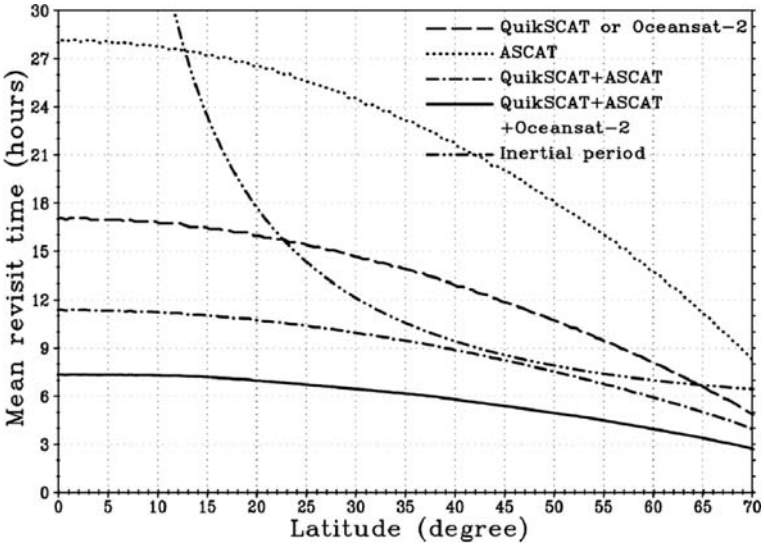

Fig. 6.9 The latitudinal variation of zonally averaged revisit interval for various tandem missions

high latitudes. Liu et al. (2008b) demonstrated that the combination of the three sensors brings the revisit interval close to 6 h from equator to the pole, meeting the 6 hourly operational NWP requirement and the inertial frequency required by the oceanographers. Because the scatterometer on Oceansat-2 has similar design as QuikSCAT, the transportability of GMF-S developed for QuikSCAT to a well-calibrated Oceansat-2 scatterometer could be tested. China is planning to launch a Ku-band scatterometer similar to QuikSCAT on the Haiyang-2 mission in 2011. Its sampling characteristic is expected to be very similar to QuikSCAT (see Liu et al., 2008b).

6.7 Discussions

It is insufficient to view the distribution of ocean surface stress by deriving it only from wind field through traditional drag coefficient. The overall large-scale difference between directly retrieved stress and stress derived from U_N may not be large, but the regional differences are significant. Our preliminary studies show the feasibility of developing a prototype GMF-S to retrieve stress from QuikSCAT observations, which we intended to proceed expeditiously when support becomes available. Processing of QuikSCAT observations for a decade long of continuous and consistent ocean surface stress field would enable the science community for new applications from a new perspective.

QuikSCAT is operating far beyond its expected life span and may fail at anytime. The transportability of such model function to a similar sensor is important. With a follow-on mission to QuikSCAT not yet confirmed, the Indian and Chinese components of a scatterometer constellation become all the more important, not only to improve the sampling of ocean surface wind and stress, but also to meet the contingency of filling any data gap.

Not all spacebased ocean surface wind and stress measurements are comparable in quality. Standardizing the technology requirements for observation accuracies of different research and operational applications and international cooperation are very desirable. Many scientific reports have affirmed the need of high quality, continuous, and consistent long time-series of ocean surface wind and stress vectors.

Acknowledgements This study was performed at the Jet Propulsion Laboratory, California Institute of Technology, under contract with the US National Aeronautics and Space Administration (NASA). It was jointly supported by the Ocean Vector Winds and the Physical Oceanography Programs of NASA.

References

Bourassa MA, Vincent DG, Wood WL (1999) A flux parameterization including the effects of capillary waves and sea state. J Atmos Sci 56:1123–1139

Chao Y, Li Z, Farrara J, McWilliams JC, Bellingham J, Capet X, Chavez F, Choi JK, Davis R, Doyle J, Frantaoni D, Li PP, Marchesiello P, Moline MA, Paduan J, Ramp S (2009)

Development, implementation and evaluation of a data-assimilative ocean forecasting system off the central California coast. Deep Sea Res II, 56:100–126
Charnock H (1955) Wind stress on a water surface. Quart J Roy Meteor Soc 81:639–640
Chelton DB, Esbensen SK, Schlax MG, Thum N, Freilich MH, Wentz FJ, Gentemann CL, McPhaden MJ, Schoff PS (2001) Observations of coupling between surface wind stress and sea surface temperature in the eastern tropical Pacific. J Clim 14:1479–1498
DeCosmo J, Katsaors KB, Smith SD, Anderson RJ, Oost WA, Bumke K, Chadwick H (1996) Air-sea exchange of water vapor and sensible heat: the humidity exchange over the sea (HEXOS) results. J Geophys Res 101:12001–12016
Donelan MA, Drenan WM, Katsaros KB (1997) The air-sea momentum flux in conditions of wind sea and swell. J Phys Oceanogr 27:2087–2099
Donelan MA, Haus BK, Reul N, Plant WJ, Stiassnie M, Graber HC, Brown OB, Saltzman ES (2004) On the limiting aerodynamic roughness of the ocean in very strong winds. Geophys Res Lett 31:L18306, doi:10.1029/2004GL019460
Donelan MA, Pierson WJ (1987) Radar scattering and equilibrium ranges in wind-generated waves with application to scatterometry. J Geophys Res 92:4971–5029
Donnelly WJ, Carswell JR, McIntosh RE, Chang PS, Wilkerson J, Marks F, Black PG (1999) Revised ocean backscatter models at C and Ku band under high-wind conditions. J Geophys Res 104:11485–11497
Emanuel K (1995) Sensitivity of tropical cyclones to surface exchange coefficients and a revised steady state model incorporating eye dynamics. J Atmos Sci 52:3969–3976
Esteban-Fernandez D, Carswell JR, Frasier S, Chang PS, Black PG, Marks FD (2006) Dual-polarized C- and Ku-band ocean backscatter response to hurricane-force winds. J Geophys Res 111:C08013, doi:10.1029/2005JC003048
Fairall CW, Bradley EF, Rogers DP, Edson JB, Young GS (1996) Bulk parameterization of air-sea fluxes in TOGA COARE. J Geophys Res 101:3747–3767
Freilich MH (1996) SeaWinds Algorithm Theoretical Basis Document. NASA ATBD-SWS-01
Fukumori I (2002) A partitioned Kalman filter and smoother. Mon Wea Rev 130:1370–1383
Hogg AMC, Dewar WK, Berloff P, Kravstov S, Hutchinson DK (2009) The effects of mesoscale ocean-atmosphere coupling on the large-scale ocean circulation. J Clim 22:4066–4082
Jones WL, Schroeder LC (1978) Radar backscatter from the ocean: dependence on surface friction velocity. Bound Layer 13:133–149
Kondo J (1975) Air-sea bulk transfer coefficients in diabetic conditions. Bound-Layer Meteor 9:91–112
Lagerloef GSE, Mitchum G, Lukas R, Niiler P (1999) Tropical Pacific near surface currents estimated from altimeter, wind and drifter data. J Geophys Res 104:23313–23326
Large WG, Pond S (1981) Open ocean momentum flux measurements in moderate to strong winds. J Phys Oceanogr 11:324–336
Lee T, Liu WT (2005) Effects of high-frequency wind sampling on simulated mixed layer depth and upper ocean temperature. J Geophys Res 110(C5):C05002, doi:10.1029/2004JC002746
Lin I-I, Liu WT, Wu CC, Chiang JC, Sui CH (2003) Satellite observations of modulation of surface winds by typhoon-induced upper ocean cooling. Geophys Res Lett 30:1131, doi:10.1029/2002GL015674
Liu WT (2002) Progress in scatterometer application. J Oceanogr 58:121–136
Liu WT (2010) Sea surface wind/stress vector. Encyclopedia of Remote Sensing, Springer, Heidelberg (in press)
Liu WT, Blanc TV (1984) The Liu, Katsaros and Businger (1979) Bulk Atmospheric Flux Computational Iteration Program in FORTRAN and BASIC. NRL Memo. Rep. 5291, Naval Research Laboratory, Washington DC, 16pp
Liu WT, Katsaros KB, Businger JA (1979) Bulk parameterization of air-sea exchanges in heat and water vapor including the molecular constraints at the interface. J Atmos Sci 36:1722–1735
Liu WT, Large WG (1981) Determination of surface stress by Seasat-SASS: a case study with JASIN Data. J Phys Oceanogr 11:1603–1611

Liu WT, Tang W (1996) Equivalent Neutral Wind, JPL Publication 96-17, Jet Propulsion Laboratory, Pasadena, California, 16pp
Liu WT, Tang W, Xie X (2008a) Wind power distribution over global ocean. Geophys Res Lett 35:L13808, doi:10.1029/2008GL034172
Liu WT, Tang W, Xie X (2010) Wind power at sea as observed from Space. In: Muyeen SM (ed.) Wind Power, Intech, Vienna (in press)
Liu WT, Tang W, Xie X, Navalgund R, Xu K (2008b) Power density of ocean surface wind-stress from international scatterometer tandem missions. Int J Remote Sens 29(21):6109–6116
Liu WT, Xie X (2006) Measuring ocean surface wind from space. In: Gower J (ed.) Remote Sensing of the Marine Environment, Manual of Remote Sensing, 3rd Edition, Vol. 6, American Society for Photogrammetry and Remote Sensing, Bethesda MD, USA, Chapter 5, pp. 149–178
Liu WT, Xie X (2008) Ocean-atmosphere momentum coupling in the Kuroshio Extension observed from Space. J Oceanogr 64:631–637
Liu WT, Xie X, Niiler PP (2007) Ocean-atmosphere interaction over Agulhas Extension Meanders. J Clim 20(23):5784–5797
Liu WT, Xie X, Polito PS, Xie S, Hashizume H (2000) Atmosphere manifestation of tropical instability waves observed by QuikSCAT and Tropical Rain Measuring Missions. Geophys Res Lett 27:2545–2548
Niiler PP (2001) Ocean circulation and climate-observing and modeling the global ocean. In: Chruch J, Siedler G, Gould J (eds.) The World Ocean Circulation, Academic Press, San Diego, pp. 193–204
Nikuradse J (1933) Stromungsgesetze in rauben Rohren. V.D.I. Forschungsheft 361:22
Nonaka M, Xie SP (2003) Covariations of sea surface temperature and wind over the Kuroshio and its extension: evidence for ocean-to-atmosphere feedback. J Clim 16:1404–1413
O'Neill LW, Chelton DB, Esbensen S (2003) Observations of SST-induced perturbations of the wind stress field over the Southern Ocean on seasonal timescales. J Clim 16: 2340–2353
Pacanowski RC (1987) Effect of equatorial currents on surface stress. J Phys Oceanogr 17:833–838
Park KA, Cornillon P (2002) Stability-induced modification of sea surface winds over Gulf Stream rings. Geophys Res Lett 29(24):2211, doi:10.1029/2001GL014236i
Park KA, Cornillon P, Codiga DL (2006) Modification of surface winds near ocean fronts: effects of the Gulf Stream rings on scatterometer (QuikSCAT, NSCAT) wind observations. J Geophys Res 111:C03021, doi:10/1029/2005JC003016
Pezzi LP, Vialard J, Richard KJ, Menkes C, Anderson D (2004) Influence of ocean-atmosphere coupling on the properties of tropical instability waves. Geophys Res Lett 31:L16306, doi:10/1029/2004GO019995
Pierson WJ (1984) A Monte-Carlo comparison of the recovery of winds near upwind and downwind from the SASS-1 model function by means of the sum of squares algorithm and a maximum likelyhood estimator. NASA Rep. 3939
Polito PS, Ryan JP, Liu WT, Chavez FP (2001) Oceanic and atmospheric anomalies of tropical instability waves. Geophys Res Lett 28:2233–2236
Powell MD, Vickery PJ, Reinhold T (2003) Reduced drag coefficient for high wind speeds in tropical cyclones. Nature 422:279–283
Seo H, Miller AJ, Roads JO (2007) The scripps coupled ocean-atmosphere regional (SCOAR) Model, with applications in the eastern Pacific sector. J Clim 20:381–402
Shaffer SJ, Dunbar RS, Hsiao SV, Long DG (1991) A median-filter-based ambiguity removal algorithm for NSCAT. IEEE Trans Geosci Rem Sens 29:167–174
Small RJ, de Szoeke S, Xie SP, O'Neill L, Seo H, Song Q, Cornillon P, Spall M, Minobe S (2008) Air–sea interaction over ocean fronts and eddies. Dyn Ocean Atmos 45:274–319
Smith SD (1980) Wind stress and heat flux over the ocean in gale force winds. J Phys Oceanogr 10:709–726
Spall MA (2007) Effect of sea surface temperature-wind stress coupling on baroclinic instability in the ocean. J Phys Oceanogr 37:1092–1097

Vecchi GA, Xie SP, Fischer AS (2004) Ocean-atmosphere covariability in the western Arabian Sea. J Clim 17:1213–1224

Weissman DE, Graber HC (1999) Satellite scatterometer studies of ocean surface stress and drag coefficient direct model. J Geophys Res 104:11329–11335

Wentz FJ (1978) Estimation of the sea surface's two-scale backscatter parameters. NASA Contractor Rep. 145255

Wentz FJ, Peteherych S, Thomas LA (1984) A model function for ocean radar cross sections at 14.6 GHz. J Geophys Res 89:3689–3704

Wentz FJ, Smith DK (1999) A model function for the ocean-normalized radar cross section at 14 GHz derived from NSCAT observations. J Geophys Res 104:11499–11514

Xie SP, Hafner J, Tanimoto Y, Liu WT, Tokinaga H, Xu H (2002) Bathymetric effect on the winter climate through the sea surface temperature in the yellow and East China seas. Geophys Res Lett 29(24):2288, doi:10.1029/2002GL015884

Xie SP, Ishiwatari M, Hashizume H, Takeuchi K (1998) Coupled ocean-atmospheric waves on the equatorial front. Geophys Res Lett 25:3863–3866

Yueh S, West R, Li F, Tsai W, Lay R (2000) Dual-polarized Ku-band backscatter signatures of hurricane ocean winds. IEEE Trans Geosci Rem Sens 38:73–88